Non-collinear itinerant magnetism: the case of Mn_3Sn

1989 J. Phys.: Condens. Matter 1 8155

(http://iopscience.iop.org/0953-8984/1/43/016)

J. Phys.: Condens. Matter 1 (1989) 8155–8170. Printed in the UK

Non-collinear itinerant magnetism: the case of Mn_3Sn

J Sticht, K-H Höck and J Kübler

Institut für Festkörperphysik, Technische Hochschule, D-6100 Darmstadt, Federal Republic of Germany

Received 20 June 1989

Abstract. Spin-density functional theory is applied to describe non-collinear itinerant magnetism. For this the theory is formulated and a new implementation is given. It serves to perform self-consistent energy-band calculations for the compound Mn_3Sn which possesses a triangular magnetic structure. Our results are discussed in detail and compared with experimental data.

1. Introduction

We have recently formulated a local approximation to density functional theory to treat non-collinear, itinerant magnetic systems and applied it to metallic compounds like γ-FeMn, $RhMn_3$, $PtMn_3$ and Mn_3GaN (Kübler *et al* 1988a, b). Although our theory was not the first to treat itinerant magnetic moments as vector observables which admit non-collinear arrangements—previous examples being work by Korenman *et al* (1977), You and Heine (1982), Oguchi *et al* (1983), Pindor *et al* (1983), Haines *et al* (1985), Sandratskii and Guletskii (1986) and Liechtenstein *et al* (1987)—we could show, for the first time, that under certain restricted symmetry conditions itinerant electrons conspire to form local magnetic moments attaining definite, non-collinear arrangements that are a property of the ground state.

We here want to discuss briefly the density functional background again taking a slightly different point of view, but suggest at some length another more powerful implementation that removes some of the drawbacks of our earlier theory. We use this implementation and apply it to the compound Mn_3Sn which experimentally shows an interesting magnetic order. The latter was discussed in detail by Nagamiya (1979) and more recently by Tomiyoshi and Yamaguchi (1982) who invoked Dzyaloshinsky–Moriya exchange interactions (Dzyaloshinsky 1958, Moriya 1960a, b) to explain the observed triangular magnetic order. Our calculations give a set of possible ground states, among them being the one observed. Since Dzyaloshinsky–Moriya exchange is brought about by a combination of spin–orbit and super-exchange interactions, we discuss spin–orbit coupling but, for technical reasons, cannot yet give results that unambiguously identify the ground-state order. Other, symmetry-adapted, non-collinear spin arrangements are calculated and found to have much higher total energies than the ground state. The reason for this is extracted from our band structure results.

0953-8984/89/438155+16$02.50

2. Theoretical background

2.1. Density functional theory

We begin by stating the theoretical framework as briefly as possible and write the total energy E as a functional of the density matrix $\boldsymbol{\rho}(\boldsymbol{r})$ (Hohenberg and Kohn 1964, Kohn and Sham 1965, von Barth and Hedin 1972, von Barth 1984):

$$E\{\boldsymbol{\rho}\} = T_0 + \sum_{\alpha\beta} \int w_{\alpha\beta}(\boldsymbol{r})\, \rho_{\beta\alpha}(\boldsymbol{r})\, \mathrm{d}^3 r + \int\int \frac{n(\boldsymbol{r}) n(\boldsymbol{r}')}{|\boldsymbol{r} - \boldsymbol{r}'|}\, \mathrm{d}^3 r\, \mathrm{d}^3 r' + E_{\mathrm{xc}}\{\boldsymbol{\rho}\} \tag{1}$$

where $\rho_{\alpha\beta}(\boldsymbol{r})$ (α and β are spin indices) are the elements of $\boldsymbol{\rho}(\boldsymbol{r})$, the particle density is

$$n(\boldsymbol{r}) = \mathrm{Tr}\, \boldsymbol{\rho}(\boldsymbol{r}) \tag{2}$$

T_0 is the kinetic energy of non-interacting electrons, E_{xc} is the exchange–correlation energy, and the units are such that the length is measured in Bohr radii and the energy in rydbergs. The external field $\mathbf{w}(\boldsymbol{r})$ is assumed to have elements $w_{\alpha\beta}(\boldsymbol{r})$ and couples to the spin-density matrix. The variational property of the total energy is well known and need not be discussed here any further; for a most recent and thorough treatment the reader may consult Vignale and Rasolt (1988). Minimisation of the total energy with respect to the elements of the density matrix yields the effective single-particle equations

$$\sum_{\beta=1}^{2} \left[-\delta_{\alpha\beta}\nabla^2 + w_{\alpha\beta}^{\mathrm{eff}}(\boldsymbol{r})\right] \psi_{\beta i}(\boldsymbol{r}) = \varepsilon_i \psi_{\alpha i}(\boldsymbol{r}) \tag{3}$$

where the effective potential is

$$w_{\alpha\beta}^{\mathrm{eff}}(\boldsymbol{r}) = w_{\alpha\beta} + 2\delta_{\alpha\beta} \int \frac{n(\boldsymbol{r}')}{|\boldsymbol{r} - \boldsymbol{r}'|}\, \mathrm{d}^3 r' + V_{\alpha\beta}^{\mathrm{xc}}(\boldsymbol{r}) \tag{4}$$

and $V_{\alpha\beta}^{\mathrm{xc}}(\boldsymbol{r})$ is the exchange–correlation potential defined by the functional derivative

$$V_{\alpha\beta}^{\mathrm{xc}}(\boldsymbol{r}) = \frac{\delta E_{\mathrm{xc}}\{\rho_{\alpha\beta}\}}{\delta \rho_{\alpha\beta}}. \tag{5}$$

If we are dealing with an N-electron system, then the elements of the density matrix are obtained from the N lowest-lying one-electron eigenfunctions of equation (3) as follows:

$$\rho_{\alpha\beta}(\boldsymbol{r}) = \sum_{i=1}^{N} \psi_{\alpha i}(\boldsymbol{r}) \psi_{\beta i}^{*}(\boldsymbol{r}). \tag{6}$$

Central to this theory is the assumed functional dependence of the exchange–correlation energy on the density matrix. Equivalent but physically more appealing is, instead, a dependence on a vector quantity describing the local spin-density vector or magnetic

moment vector. To obtain this we observe that at each point in space we can find a transformation matrix $\mathbf{U}(\boldsymbol{r})$ with elements $U_{i\alpha}(\boldsymbol{r})$ such that

$$\sum_{\alpha\beta} U_{i\alpha}(\boldsymbol{r})\rho_{\alpha\beta}(\boldsymbol{r})U^{+}_{\beta j}(\boldsymbol{r}) = \delta_{ij}n_i(\boldsymbol{r}) \tag{7}$$

is diagonal; $n_i(\boldsymbol{r})$ $(i = 1,2)$ denote the eigenvalues of $\boldsymbol{\rho}(\boldsymbol{r})$. For the matrix $\mathbf{U}(\boldsymbol{r})$ we choose the well known spin $-\frac{1}{2}$ rotation matrix,

$$\mathbf{U}(\boldsymbol{r}) = \begin{pmatrix} \exp\left(\frac{1}{2}\mathrm{i}\varphi(\boldsymbol{r})\right)\cos\left(\frac{1}{2}\theta(\boldsymbol{r})\right) & \exp\left(-\frac{1}{2}\mathrm{i}\varphi(\boldsymbol{r})\right)\sin\left(\frac{1}{2}\theta(\boldsymbol{r})\right) \\ -\exp\left(\frac{1}{2}\mathrm{i}\varphi(\boldsymbol{r})\right)\sin\left(\frac{1}{2}\theta(\boldsymbol{r})\right) & \exp\left(-\frac{1}{2}\mathrm{i}\varphi(\boldsymbol{r})\right)\cos\left(\frac{1}{2}\theta(\boldsymbol{r})\right) \end{pmatrix}$$

and obtain with the requirement expressed by equation (7) the polar angles ϕ, θ at each point in space as follows

$$\tan\varphi(\boldsymbol{r}) = -\frac{\operatorname{Im}\rho_{12}(\boldsymbol{r})}{\operatorname{Re}\rho_{12}(\boldsymbol{r})} \tag{8a}$$

$$\tan\theta(\boldsymbol{r}) = 2[(\operatorname{Re}\rho_{12}(\boldsymbol{r}))^2 + (\operatorname{Im}\rho_{12}(\boldsymbol{r}))^2]^{1/2}/(\rho_{11}(\boldsymbol{r}) - \rho_{22}(\boldsymbol{r})). \tag{8b}$$

Furthermore, using equation (7) to express the functional derivatives $\delta E_{\mathrm{xc}}/\delta\rho_{\alpha\beta}$ in terms of $\delta E_{\mathrm{xc}}/\delta n_i$, we straightforwardly obtain the effective potential $\mathbf{w}^{\mathrm{eff}}(\boldsymbol{r})$ (whose elements are the $w^{\mathrm{eff}}_{\alpha\beta}(\boldsymbol{r})$ of equation (4)) as follows

$$\mathbf{w}^{\mathrm{eff}}(\boldsymbol{r}) = v_0(\boldsymbol{r})\mathbf{I} + \Delta v(\boldsymbol{r})\tilde{\boldsymbol{\sigma}}^z(\boldsymbol{r}). \tag{9}$$

Here $v_0(\boldsymbol{r})$ is the spin-independent part of the effective potential given by

$$v_0(\boldsymbol{r}) = v(\boldsymbol{r}) + 2\int \frac{n(\boldsymbol{r}')}{|\boldsymbol{r}-\boldsymbol{r}'|}\,\mathrm{d}^3r' + \frac{1}{2}\sum_{i=1}^{2}\frac{\delta E_{\mathrm{xc}}}{\delta n_i} \tag{10}$$

where $v(\boldsymbol{r})$ is the nuclear potential, the quantity $\Delta v(\boldsymbol{r})$ is given by

$$\Delta v(\boldsymbol{r}) = \frac{1}{2}\left(\frac{\delta E_{\mathrm{xc}}}{\delta n_1} - \frac{\delta E_{\mathrm{xc}}}{\delta n_2}\right) \tag{11}$$

and $\tilde{\boldsymbol{\sigma}}^z(\boldsymbol{r})$ is the z component of the Pauli spin matrix in a reference frame which is the standard representation rotated by $\theta(\boldsymbol{r})$ and $\phi(\boldsymbol{r})$, i.e.

$$\tilde{\boldsymbol{\sigma}}^z(\boldsymbol{r}) = \mathbf{U}^{+}(\boldsymbol{r})\boldsymbol{\sigma}^z(\boldsymbol{r})\mathbf{U}(\boldsymbol{r}) = \cos\theta(\boldsymbol{r})\boldsymbol{\sigma}^z + \sin\theta(\boldsymbol{r})(\cos\varphi(\boldsymbol{r})\boldsymbol{\sigma}^x + \sin\varphi(\boldsymbol{r})\boldsymbol{\sigma}^y). \tag{12}$$

In terms of the above variables the effective single-particle equation (3) becomes

$$\sum_{\beta=1}^{2}[\delta_{\alpha\beta}(-\nabla^2 + v_0(\boldsymbol{r})) + \Delta v(\boldsymbol{r})\tilde{\sigma}^z_{\alpha\beta}(\boldsymbol{r})]\psi_{\beta i}(\boldsymbol{r}) = \varepsilon_i\psi_{\alpha i}(\boldsymbol{r}) \qquad \alpha = 1,2. \tag{13}$$

As normal with density functional theory the calculation needs to be made self-consistent, a requirement which besides charge density, $n(\boldsymbol{r}) = n_1(\boldsymbol{r}) + n_2(\boldsymbol{r})$, and magnitude of the local magnetisation density, $m(\boldsymbol{r}) = n_1(\boldsymbol{r}) - n_2(\boldsymbol{r})$, now also applies to the direction of the magnetic moment, i.e. the angles (and starting quantities) in the

potential $\Delta v(\boldsymbol{r})\,\tilde{\sigma}^z_{\alpha\beta}(\boldsymbol{r})$, see equation (12), which supplies the wavefunctions with equation (13); these in turn yield the density matrix and through its diagonalisation output angles $\theta(\boldsymbol{r})$ and $\phi(\boldsymbol{r})$, equation (8). Although this appears quite plausible one might still ask whether the self-consistency condition is really necessary. For an answer we may follow Vignale and Rasolt (1988) and expand the potentials as well as the density matrix in terms of Pauli matrices (in the standard representation), i.e.

$$w_{\alpha\beta}(\boldsymbol{r}) = w(\boldsymbol{r})\delta_{\alpha\beta} + \sum_{\lambda=1}^{3} w_\lambda(\boldsymbol{r})\sigma^\lambda_{\alpha\beta} \tag{14a}$$

$$V^{\mathrm{xc}}_{\alpha\beta}(\boldsymbol{r}) = V^{\mathrm{xc}}(\boldsymbol{r})\delta_{\alpha\beta} + \sum_{\lambda=1}^{3} V^{\mathrm{xc}}_\lambda(\boldsymbol{r})\sigma^\lambda_{\alpha\beta} \tag{14b}$$

and

$$\rho_{\alpha\beta}(\boldsymbol{r}) = \rho(\boldsymbol{r})\delta_{\alpha\beta} + \sum_{\lambda=1}^{3} \rho_\lambda(\boldsymbol{r})\sigma^\lambda_{\alpha\beta}. \tag{14c}$$

Then from the *exact* Hamiltonian the continuity equations in the ground state are easily derived:

$$\nabla \boldsymbol{j}_p(\boldsymbol{r}) = 0 \tag{15}$$

$$\nabla \boldsymbol{j}_{p\lambda}(\boldsymbol{r}) = 2(\boldsymbol{w} \times \boldsymbol{\rho})_\lambda \tag{16}$$

where $\boldsymbol{j}_p$ is the paramagnetic current density and $\boldsymbol{j}_{p\lambda}$ its expansion analoguous to equation (14*c*); i.e.

$$\boldsymbol{j}_{p\alpha\beta}(\boldsymbol{r}) = -\frac{i}{2}\sum_{i=1}^{N}\{\psi^*_{i\beta}(\boldsymbol{r})\nabla\psi_{i\alpha}(\boldsymbol{r}) - [\nabla\psi_{i\beta}(\boldsymbol{r})]^*\psi_{i\alpha}(\boldsymbol{r})\}. \tag{17a}$$

and

$$\boldsymbol{j}_{p\alpha\beta}(\boldsymbol{r}) = \boldsymbol{j}_p(\boldsymbol{r})\delta_{\alpha\beta} + \sum_{\lambda=1}^{3} \boldsymbol{j}_{p\lambda}(\boldsymbol{r})\sigma^\lambda_{\alpha\beta}. \tag{17b}$$

The quantities $\boldsymbol{w}$ and $\boldsymbol{\rho}$ denote vectors spanned by the components w_λ and ρ_λ, equations (14), and we assumed a zero external vector potential. Requiring equation (16) also to hold for the solutions of the single-particle equation (3), we obtain

$$(\boldsymbol{V}^{\mathrm{xc}} \times \boldsymbol{\rho}) = 0 \tag{18}$$

i.e. the vector quantities $\boldsymbol{V}^{\mathrm{xc}}$ and $\boldsymbol{\rho}$ must be parallel if they are non-zero. This is equivalent to the above-mentioned self-consistency condition (because input angles characterise $\boldsymbol{V}^{\mathrm{xc}}$ and output angles $\boldsymbol{\rho}$). But, Vignale and Rasolt (1988) show more: their equation (6.10*b*) indeed admits solutions with

$$(\boldsymbol{V}^{\mathrm{xc}} \times \boldsymbol{\rho}) \neq 0$$

which they show to be a consequence of gauge invariance; however, in this case, a finite 'exchange–correlation vector potential' as well as currents must be included in the theory, which means that the dependence of the exchange–correlation energy on the paramagnetic currents, equation (16), can no longer be ignored. This, however, is beyond the scope of our present theory.

Returning to the self-consistent-field problem embodied in equation (13) we state two approximations without which this theory remains largely academic. The first is the well known local approximation to density functional theory where we write the exchange–correlation energy as

$$E_{\mathrm{xc}}\{n_1, n_2\} = \int n(\boldsymbol{r})\epsilon_{\mathrm{xc}}\left[n_1(\boldsymbol{r}), n_2(\boldsymbol{r})\right] \mathrm{d}^3 r \tag{19}$$

and interpret the dependence of ϵ_{xc} to be on the eigenvalues $n_1(\boldsymbol{r})$ and $n_2(\boldsymbol{r})$ of the density matrix. The second concerns the dependence of the angles θ and ϕ on space, $\boldsymbol{r}$, i.e. the direction of local magnetisation. Here we make the atomic-sphere approximation and assume that at each point within a given sphere the local direction of magnetisation is the same, allowing, however, for different directions in different spheres. This way we replace a fine-grained mesh by a coarse-grained mesh and consequently use θ^{ν} and ϕ^{ν} instead of $\theta(\boldsymbol{r})$ and $\phi(\boldsymbol{r})$ labelling with ν the type of atomic sphere. Similarly, the unitary transformation defined by $\mathbf{U}(\boldsymbol{r})$ now becomes $\mathbf{U}^{\nu}$ which is assumed to diagonalise the density matrix integrated over the atomic sphere, S_{ν}; i.e. if one defines

$$q^{\nu}_{\alpha\beta} \doteq \int_{S_{\nu}} \rho_{\alpha\beta}(\boldsymbol{r})\, \mathrm{d}^3 r \tag{20}$$

then

$$\sum_{\alpha\beta} U^{\nu}_{i\alpha} q^{\nu}_{\alpha\beta} U^{\nu^{+}}_{\beta j} = q^{\nu}_{i}\delta_{ij}. \tag{21}$$

Finally, as we showed earlier (Kübler *et al* 1988a), the total energy is easily obtained as follows:

$$E = \sum_{i=1}^{N} \varepsilon_i - \int\int \frac{n(\boldsymbol{r})n(\boldsymbol{r}')}{|\boldsymbol{r}-\boldsymbol{r}'|}\, \mathrm{d}^3 r\, \mathrm{d}^3 r' - \sum_{\alpha=1}^{2} \int n(\boldsymbol{r})\, \frac{\partial \epsilon_{\mathrm{xc}}}{\partial n_{\alpha}}\, n_{\alpha}(\boldsymbol{r})\, \mathrm{d}^3 r \tag{22}$$

where, for $\boldsymbol{r}$ in the atomic sphere ν, $n_{\alpha}(\boldsymbol{r})$ denotes the diagonal elements of $\mathbf{U}^{\nu}\,\boldsymbol{\rho}(\boldsymbol{r})\,\mathbf{U}^{\nu^{+}}$; thus the spin-density in the νth atomic sphere is

$$m(\boldsymbol{r}) = n_1(\boldsymbol{r}) - n_2(\boldsymbol{r})$$

giving a magnetic moment (in μ_{B}) of

$$\mu^{\nu} = q^{\nu}_1 - q^{\nu}_2.$$

2.2. Implementation

The implementation that we will describe here is different from our earlier one (Kübler *et al* 1988a) and is more precise. The reason is that the basis functions which we use to expand the Bloch functions are numerical solutions of the locally diagonal *spin-dependent* Schrödinger equation whereas previously we used basis functions that locally solved a Schrödinger equation containing the spin-independent potential $v_0(\boldsymbol{r})$, equation (10), only. We believe this better implementation is essential when dealing with rather large magnetic moments as we will do in the next section.

Let us begin by defining the two-component basis functions $\Xi_L^\nu(\boldsymbol{r})$, where ν labels the νth atomic sphere that is also assumed to contain the origin of $\boldsymbol{r}$, through the equation

$$[(-\nabla^2 + v_0^\nu(\boldsymbol{r}))\mathbf{I} + \Delta v^\nu(\boldsymbol{r})\boldsymbol{\sigma}^z]\Xi_L^\nu(\boldsymbol{r}) = E_L^\nu\,\Xi_L^\nu(\boldsymbol{r}) \tag{23}$$

where $v_0^\nu(\boldsymbol{r})$ and $\Delta v^\nu(\boldsymbol{r})$ are defined by equations (10) and (11) in the νth atomic sphere, $\boldsymbol{\sigma}^z$ is the z component of the Pauli spin matrix in the standard representation and, as usual, $L = (l, m)$ labels the angular momentum l and magnetic quantum number m. The function Ξ is the product of a spinor function χ^σ, where

$$\boldsymbol{\sigma}^z\chi^\sigma = \sigma\chi^\sigma \tag{24}$$

$\sigma = \pm 1$, with an $\boldsymbol{r}$-dependent function $\xi_L^{\nu\sigma}(\boldsymbol{r})$ defined by

$$[-\nabla^2 + v_0^\nu(\boldsymbol{r}) + \sigma\Delta v^\nu(\boldsymbol{r})]\xi_L^{\nu\sigma}(\boldsymbol{r}) = E_L^{\nu\sigma}\,\xi_L^{\nu\sigma}(\boldsymbol{r}) \tag{25}$$

and is thus a basis function solving the locally diagonal spin-dependent Schrödinger equation. If we specify the direction of the magnetic moment in the νth atomic sphere by means of the polar angles θ^ν and ϕ^ν with respect to some global axis, then we need solutions of the spin-coupled differential equation

$$[(-\nabla^2 + v_0^\nu(\boldsymbol{r}))\mathbf{I} + \Delta v^\nu(\boldsymbol{r})\tilde{\boldsymbol{\sigma}}^{\nu z}]\Psi_L^\nu(\boldsymbol{r}) = E_L^\nu\,\Psi_L^\nu(\boldsymbol{r}) \tag{26}$$

where $\tilde{\boldsymbol{\sigma}}^{\nu z}$ is given by equation (12), but $\boldsymbol{r}$ is replaced by the label ν. Now, obviously,

$$\Psi_L^\nu(\boldsymbol{r}) = \mathbf{U}^{\nu^-}\,\Xi_L^\nu(\boldsymbol{r}) \tag{27}$$

and for each L and ν there are two solutions which we write in terms of those of equation (25)

$$\Psi_L^{\nu\sigma}(\boldsymbol{r}) = \xi_L^{\nu\sigma}(\boldsymbol{r})\,\chi^{\nu,\sigma} \tag{28}$$

where $\sigma = \pm 1$ and the 'rotated' spinor functions, $\chi^{\nu,\sigma}$, are

$$\chi^{\nu,+1} = (U_{11}^\nu)^*\chi^{+1} + (U_{12}^\nu)^*\chi^{-1} \tag{29a}$$

and

$$\chi^{\nu,-1} = (U_{21}^\nu)^*\chi^{+1} + (U_{22}^\nu)^*\chi^{-1}. \tag{29b}$$

Our definition of the basis functions is not yet complete and depends on the method used to solve the crystal Schrödinger equation, i.e. on the type of expansion used for the Bloch functions. In the augmented spherical wave (ASW) method (Williams *et al* 1979), we require at the radius, S_ν, of the νth atomic sphere the solutions, ξ, of equation (25), to match the value and slope of a spin-independent spherical Hankel function, $h_{L\nu}(\boldsymbol{r})$, of some small energy ($E_0 = -0.01$ Ryd for convenience), centred at site ν. We call these solutions of the eigenvalue equation (24) 'augmented' Hankel functions, denoting them by $\tilde{h}_{L\nu\sigma}$ with eigenvalue $E^{\mathrm{H}}_{L\nu\sigma}$; an augmented Hankel function, centred at $\boldsymbol{R}_j + \boldsymbol{\tau}_\nu$ in the crystal is then defined by

$$\eta_{L\nu\sigma}(\boldsymbol{r} - \boldsymbol{R}_j - \boldsymbol{\tau}_\nu) = \begin{cases} \tilde{h}_{L\nu\sigma}(\boldsymbol{r} - \boldsymbol{R}_j - \boldsymbol{\tau}_\nu)\chi^{\nu,\sigma} & \text{if } |\boldsymbol{r} - \boldsymbol{R}_j - \boldsymbol{\tau}_\nu| < S_\nu \\ h_{L\nu}(\boldsymbol{r} - \boldsymbol{R}_j - \boldsymbol{\tau}_\nu)\chi^{\nu,\sigma} & \text{otherwise} \end{cases} \qquad \sigma = \pm 1. \quad (30)$$

The advantage of the spherical Hankel functions is the well known KKR theorem (Korringa 1947, Kohn and Rostoker 1954) which allows their expansion about any other centre in terms of spherical Bessel functions, $j_{L\nu}(\boldsymbol{r})$, i.e. if $\boldsymbol{r}$ is such that $|\boldsymbol{r} - \boldsymbol{R}_i - \boldsymbol{\tau}_\mu| < S_\mu$, then for $\boldsymbol{R}_j$, $\boldsymbol{\tau}_\nu$ other than $\boldsymbol{R}_i$, $\boldsymbol{\tau}_\mu$

$$h_{L\nu}(\boldsymbol{r} - \boldsymbol{R}_j - \boldsymbol{\tau}_\nu) = \sum_{L'} B^{\nu\mu}_{LL'}(\boldsymbol{R}_j - \boldsymbol{R}_i)\, j_{L'\mu}(\boldsymbol{r} - \boldsymbol{R}_i - \boldsymbol{\tau}_\mu) \quad (31)$$

where the $B^{\nu\mu}_{LL'}(\boldsymbol{R})$ are the well known KKR 'structure' factors (whose dependence on energy we suppressed in the notation). The spherical Bessel functions supply another set of boundary conditions for equation (25) just like the spherical Hankel functions. We call them augmented Bessel functions, they have the energy $E^J_{L\nu\sigma}$, and are denoted by $\tilde{j}_{L\nu\sigma}(\boldsymbol{r})$; again, a two-component augmented Bessel functions centred at $\boldsymbol{R}_i + \boldsymbol{\tau}_\mu$ is then defined by

$$\zeta_{L\mu\sigma}(\boldsymbol{r} - \boldsymbol{R}_i - \boldsymbol{\tau}_\mu) = \begin{cases} \tilde{j}_{L\mu\sigma}(\boldsymbol{r} - \boldsymbol{R}_i - \boldsymbol{\tau}_\mu)\chi^{\mu,\sigma} & \text{if } |\boldsymbol{r} - \boldsymbol{R}_i - \boldsymbol{\tau}_\mu| < S_\mu \\ j_{L\mu}(\boldsymbol{r} - \boldsymbol{R}_i - \boldsymbol{\tau}_\mu)\chi^{\mu,\sigma} & \text{otherwise} \end{cases} \qquad \sigma = \pm 1. \quad (32)$$

The KKR expansion theorem, equation (31), is now readily generalised to the unaugmented two-component functions as follows: if $\boldsymbol{r}$ is such that $|\boldsymbol{r} - \boldsymbol{R}_i - \boldsymbol{\tau}_\mu| < S_\mu$, then for $\boldsymbol{R}_j$, $\boldsymbol{\tau}_\nu$ other than $\boldsymbol{R}_i$, $\boldsymbol{\tau}_\mu$

$$h_{L\mu}(\boldsymbol{r} - \boldsymbol{R}_j - \boldsymbol{\tau}_\nu)\chi^{\nu,\sigma} = \sum_{L'\sigma'} G^{\nu\mu}_{L\sigma L'\sigma'}(\boldsymbol{R}_j - \boldsymbol{R}_i)\, j_{L'\mu}(\boldsymbol{r} - \boldsymbol{R}_i - \boldsymbol{\tau}_\mu)\, \chi^{\mu,\sigma'} \quad (33)$$

where

$$G^{\nu\mu}_{L\sigma L'\sigma'}(\boldsymbol{R}) = B^{\nu\mu}_{LL'}(\boldsymbol{R}) T^{\nu\mu}_{\sigma'\sigma} \quad (34)$$

and $T^{\nu\mu}_{\sigma'\sigma}$ are the matrix elements of

$$\mathbf{T}^{\nu\mu} = \mathbf{U}^{\mu}\mathbf{U}^{\nu+}. \quad (35)$$

For the augmented functions we therefore obtain

$$\eta_{L\nu\sigma}(\boldsymbol{r} - \boldsymbol{R}_j - \boldsymbol{\tau}_\nu) = \begin{cases} \tilde{h}_{L\nu\sigma}(\boldsymbol{r} - \boldsymbol{R}_j - \boldsymbol{\tau}_\nu)\chi^{\nu,\sigma} & \text{if } |\boldsymbol{r} - \boldsymbol{R}_j - \boldsymbol{\tau}_\nu| < S_\nu \\ \displaystyle\sum_{L'\sigma'} G^{\nu\mu}_{L\sigma L'\sigma'}(\boldsymbol{R}_j - \boldsymbol{R}_i)\zeta_{L'\mu\sigma'}(\boldsymbol{r} - \boldsymbol{R}_i - \boldsymbol{\tau}_\mu) & \text{if } |\boldsymbol{r} - \boldsymbol{R}_i - \boldsymbol{\tau}_\mu| < S_\mu \end{cases}. \quad (36)$$

The structure factors G now contain information about both the crystal *and* the magnetic structure. They describe how the 'tail' of a two-component augmented Hankel function that is centred at some site in the crystal, having a well defined spin direction there with respect to some global frame of reference, appears at some other site with different spin direction as a linear combination of two-component augmented Bessel functions. Equation (36) finally serves to expand the Bloch function as

$$\psi_{\boldsymbol{k}}(\boldsymbol{r}) = \sum_{L\nu\sigma} C_{L\nu\sigma}(\boldsymbol{k}) \sum_{j} \exp(\mathrm{i}\boldsymbol{k}\cdot\boldsymbol{R}_j)\, \eta_{L\nu\sigma}(\boldsymbol{r}-\boldsymbol{R}_j-\boldsymbol{\tau}_\nu) \tag{37}$$

where $\boldsymbol{k}$ is a vector in the Brillouin zone and the coefficients $C_{L\nu\sigma}(\boldsymbol{k})$ are obtained from a Rayleigh–Ritz variational treatment of the effective one-particle Hamiltonian

$$\mathbf{H} = (-\nabla^2 + v_0(\boldsymbol{r}))\mathbf{I} + \Delta v(\boldsymbol{r})\tilde{\boldsymbol{\sigma}}^z \tag{38}$$

where v_0, Δv and $\tilde{\boldsymbol{\sigma}}^z$ have been defined above. The determination of the Hamiltonian and overlap matrices proceeds exactly as described before by Williams *et al* (1979), now with a spin degree of freedom added. If the latter are formally included in the notation for L, which we temporarily may replace by $\mathscr{L} = (l, m, \sigma)$, then the Hamiltonian and overlap matrices are unchanged except for the replacements of L by $\mathscr{L}$ and B by G, cf Williams *et al* (1979) equation (29).

We end this section with a remark about the construction of the charge density. When the coefficients $C_{L\nu\sigma}(k)$ and the corresponding band energies $E(k)$ are determined (condensing the notation for the band index and wavevector $\boldsymbol{k}$ into the symbol k), we obtain the elements of the integrated density matrix, $q^{\nu}_{\sigma\sigma'}$, equation (20), from the density-of-states matrix $N^{\nu}_{L\sigma\sigma'}(E)$ by means of

$$q^{\nu}_{\sigma\sigma'} = \sum_{L} \int_{-\infty}^{E_{\mathrm{F}}} N^{\nu}_{L\sigma\sigma'}(E)\, \mathrm{d}E \tag{39}$$

where the integrand follows from

$$\begin{aligned} N^{\nu}_{L,\sigma\sigma'}(E) = \sum_{k} \delta(E - E(k))\, [&C^{*}_{L\nu\sigma}(k) \langle \tilde{h}_{L\nu\sigma} \mid \tilde{h}_{L\nu\sigma'} \rangle_{\nu} C_{L\nu\sigma'}(k) \\ &+ C^{*}_{L\nu\sigma}(k) \langle \tilde{h}_{L\nu\sigma} \mid \tilde{j}_{L\nu\sigma'} \rangle_{\nu} \mathscr{A}_{L\nu\sigma'}(k) + \mathscr{A}^{*}_{L\nu\sigma}(k) \langle \tilde{j}_{L\nu\sigma} \mid \tilde{h}_{L\nu\sigma'} \rangle_{\nu} C_{L\nu\sigma'}(k) \\ &+ \mathscr{A}^{*}_{L\nu\sigma}(k) \langle \tilde{j}_{L\nu\sigma} \mid \tilde{j}_{L\nu\sigma'} \rangle_{\nu} \mathscr{A}_{L\nu\sigma'}(k)] \end{aligned} \tag{40}$$

where

$$\mathscr{A}_{L\nu\sigma}(k) = \sum_{L'\nu'\sigma'} G^{\nu'\nu}_{L'\sigma'L\sigma}(\boldsymbol{k})\, C_{L'\nu'\sigma'}(k). \tag{41}$$

and the symbol $\langle \ldots \mid \ldots \rangle_{\nu}$ denotes an integral over the νth atomic sphere the arguments being augmented Hankel, $\tilde{h}$, or Bessel functions, $\tilde{j}$. (Strictly speaking there is a factor near unity multiplying the bracket under the sum in equation (40); it serves to normalise the charge from each state and corrects for the atomic-sphere approximation.) The quantity $q^{\nu}_{\sigma\sigma'}$ is subsequently diagonalised for each atomic sphere ν giving a local

direction of magnetisation for each v and the matrices $\mathbf{U}^v$. The latter are used to construct a diagonal density-of-states matrix

$$\hat{N}^v_{L\sigma}(E) = \sum_{\sigma'\sigma''} U^v_{\sigma\sigma'} N^v_{L\sigma'\sigma''}(E)\, U^{v+}_{\sigma''\sigma} \tag{42}$$

which is all that is needed to construct the charge density for spin-up and spin-down electrons in the local (diagonal) frame of reference, see Williams *et al* (1979), thereby closing the self-consistency cycle. The magnitude of the magnetic moment (in μ_B) of the atom v is, finally,

$$\mu^v = \left| \sum_{L,\sigma} \int_{-\infty}^{E_F} \sigma \hat{N}^v_{L\sigma}(E)\, \mathrm{d}E \right|. \tag{43}$$

3. Results for Mn_3Sn

The intermetallic compound Mn_3Sn has the hexagonal crystal structure DO_{19} of space group D^4_{6h}; it has two formula units in the unit cell and is illustrated in figure 1. The lattice parameters are given by Tomiyoshi (1982) as $a = 5.665$ Å and $c/a = 0.7998$. A free-position parameter allowed by the DO_{19} structure is the distance between neighbouring Mn atoms in the same plane, which is denoted by $a[\frac{1}{2} + 3(x - \frac{5}{6})]$; Tomiyoshi (1982) gives $x = \frac{5}{6} + 0.0055$. We used these parameters for our calculations rather than trying to obtain them from the minimum of the total energy.

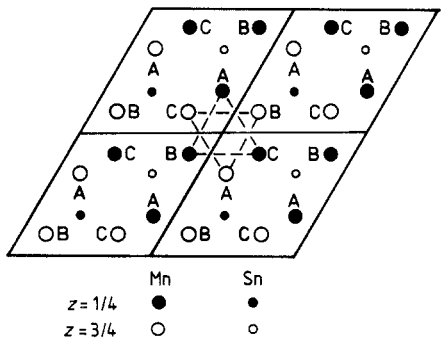

Figure 1. Basal plane projection of four unit cells of the DO_{19} crystal structure of Mn_3Sn. Magnetic sublattices are labelled A, B and C (Kouvel and Kasper 1964).

Below a Néel temperature of $T_N = 420$ K magnetic order is found which is certainly non-collinear but, when it comes to details, is discussed quite controversially, see Tomiyoshi (1982), Tomiyoshi and Yamaguchi (1982) and references therein, and most recently Tomiyoshi *et al* (1987) and Ohmori *et al* (1987).

We want to contribute to this discussion (without being able to resolve it) and start by considering all possibilities that are allowed by symmetry. In what follows we will describe these possibilities using the c axis and the planes depicted in figure 1 as

Table 1. The magnetic structures possible in DO_{19} compounds, after Zimmer and Krén (1972). The notation is that of Koster *et al* (1963).

No	Representation	Structure	Orientation	Magnetic space group
1	Γ_2^+ (Γ_4^-)		$\parallel c$	*$P6_3mm'c'$ ($P6'_3mm'c$)
2	Γ_3^+ (Γ_1^-)		$\perp c$	$P6'_3m'm'c$ ($P6_3m'm'c'$)
3	Γ_4^+ (Γ_2^-)	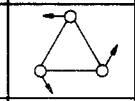	$\perp c$	$P6'_3m'mc'$ ($P6_3m'mc$)
4	Γ_5^+ (Γ_6^-)	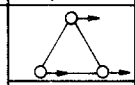	$\perp c$	*$Pm'ma'$ ($Pm'ma$)
5		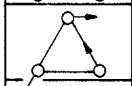		
6		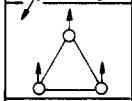	$\perp c$	*$Pm'm'a$ ($Pm'm'a'$)
7		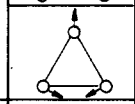		
8	Γ_6^+ (Γ_5^-)	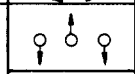	$\parallel c$	*$Pmm'a'$ ($Pmm'a$)
9		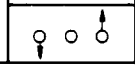		$Pmma$ ($Pmma'$)

a frame of reference. This is only done so for convenience: since the spin frame of reference is not coupled with the crystal axes, all that is important in the present paper is the relative orientation of the spins. This will change when spin–orbit coupling is included in the theory; calculations along these lines are in progress.

To enumerate the possible magnetic structures we refer to the vector notation introduced in equations (14) and find those irreducible representations of the space group D_{6h}^4 that give a non-vanishing axial vector $\boldsymbol{\rho}$ for the six Mn sites. The symmetry arguments necessary for this were carried out by Zimmer and Krén (1972) whose results are collected in table 1. Choosing one of these representations for the exchange–correlation potential $\boldsymbol{V}^{xc}$ we recover the same representation for $\boldsymbol{\rho}$ and

$$\sum_{v=1}^{6} \int_{S_v} \boldsymbol{V}^{xc}(\boldsymbol{r}) \cdot \boldsymbol{\rho}(\boldsymbol{r})\, \mathrm{d}^3 r$$

is an invariant, where the sum on v extends over the atomic spheres. This is, of course, the self-consistency condition. In table 1 the moment directions for only three Mn atoms and one Sn atom in each basal plane are sketched since the moments of corresponding atoms in adjacent planes can only be parallel or antiparallel. For the latter case the symbol of the representation and the operations of the magnetic space group are given in parantheses.

Our numerical calculations verify that the configurations given in table 1 are the only self-consistent ones; those corresponding to No 2 are depicted for adjacent planes in figure 2, see Γ_3^+ and Γ_1^-, which show the centre portion of figure 1 with the direction

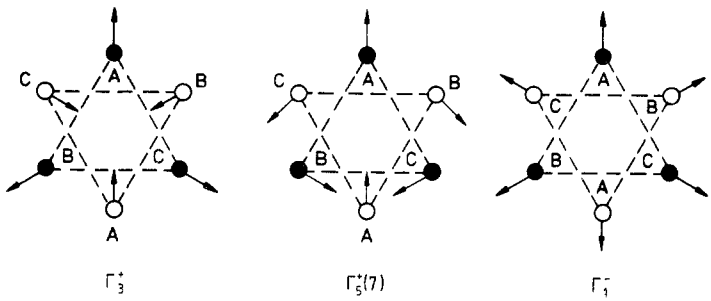

Figure 2. Some magnetic-moment arrangements of the six Mn atoms in the unit cell, labels are those defined in table 1.

of magnetisations included. One can continuously go from state Γ_3^+ to Γ_1^- if one is willing to go through a set of non-self-consistent states. The results for such a calculation are shown in figure 3(*a*), where we give the total-energy difference per unit cell (two formula units) as a function of the (input) angles ϕ needed to rotate the directions of one plane of Mn atoms. Figure 3(*b*) shows that the antiferromagnetic non-collinear state Γ_3^+ has lowest total energy and the state Γ_1^- is metastable. Also shown in figure 3(*b*) are the total-energy differences of some other self-consistent states obtained by separate calculations: the next state above the ground state has a ferromagnetic component; it is collinear and of symmetry Γ_6^+ corresponding to No 8 of table 1; following this is the collinear antiferromagnetic state Γ_4^- (No 1), still higher is the collinear ferromagnetic state Γ_2^+ (No 1), the highest being the non-collinear antiferromagnetic state Γ_1^- (No 2).

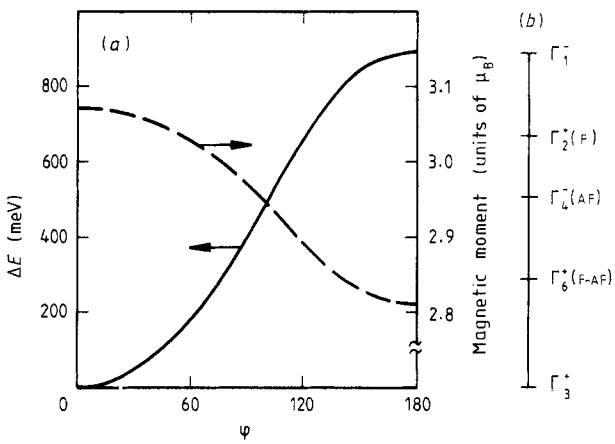

Figure 3. (*a*) Total-energy differences per unit cell and Mn magnetic moments as a function of the angle ϕ leading from the state $\Gamma_3^+(\phi = 0°)$ to $\Gamma_1^-(\phi = 120°)$. (*b*) Total-energy differences per unit cell of some other states defined in table 1.

The magnetic moment of Mn in this compound is calculated to be $2.95\mu_B \pm 5\%$, the difference, $\pm 5\%$, being in no way random but depending on the state in question. Thus, figure 3(*a*) also shows the magnetic moment as a function of ϕ going from the state Γ_3^+ with $3.07\mu_B$ to Γ_1^- with $2.82\mu_B$. In table 2 we collect the values of the

calculated magnetic moments for all states given in table 1 (except for No 9 which we are unable to prepare) and, besides the total-energy differences, list the states that are equivalent in our theory (the latter being due presumably to our neglecting the spin–orbit interaction).

Table 2. List of possible states, total energy difference, ΔE, counted from that of state Γ_3^+, in meV per unit cell, and magnetic moment of Mn in units of μ_B. (Moment of Sn negligible throughout.)

States from table 1	ΔE (meV)	Mn moment (μ_B)
Γ_3^+, Γ_4^+, Γ_5^+ (No 7), Γ_5^+ (No 5)	0	3.07
Γ_6^+ (No 8)	287	2.93†
Γ_4^-, Γ_6^- (No 4), Γ_6^- (No 6)	511	2.77
Γ_2^+, Γ_5^+ (No 4), Γ_5^+ (No 6)	697	3.07
Γ_1^-, Γ_2^-, Γ_6^- (No 7)	892	2.82

† Average value.

Finally, in view of the experimental results to be discussed in the next section, it is of interest to probe some low-lying states with a ferromagnetic component. Without a magnetic field there are no such self-consistent states near the ground state, but, ignoring self-consistency, one can go from state Γ_3^+ to the degenerate state Γ_5^+ (No 7) via the state Γ_6^+ (No 8) (called F–AF here) by changing the spin directions of atoms B and C from $\phi = 0°$ to $\phi = 120°$, compare Γ_5^+ (No 7) and Γ_3^+ in figure 2. Note that in this case (F–AF) the state Γ_6^+ as described in table 1 (No 8) is not really the one used here since all spins remain in the plane $\perp c$. The results of this calculation are shown in figure 4 where both the total-energy differences per unit cell and the Mn magnetic moments are given as a function of the input angle ϕ.

We next want to compare our results with experimental data, discuss them and try to expose the physical mechanism that is operating to stabilise the ground state among all the other states.

4. Discussion

It appears that stoichiometric samples of Mn_3Sn are very hard to prepare, so we must be content with data from samples with excess Mn atoms having a composition that is stated to range from $Mn_{3.2}Sn$ to $Mn_{3.6}Sn$. Reference to very early work can be found in Tomiyoshi (1982). His analysis of polarised-neutron diffraction data using the Mn^{2+} magnetic form factor and a magnetic structure corresponding to the state Γ_5^+ (No 7) (see table 2 and figure 2) gives a value for the magnetic moment of $1.78\mu_B$/Mn at 293 K which he extrapolates to $T = 0$ K using the Brillouin function of $S = 1$ obtaining $2.1\mu_B$/Mn. Although his magnetic structure is indeed one of the possible calculated ground states, his magnetic moment is considerably smaller than our value of $\sim 3\mu_B$/Mn. We therefore asked whether our spin density could be inconsistent with the neutron data and calculated the magnetic form factor (Lovesey 1984) using the spin density of the state Γ_5^+ (No 7). The result is shown in figure 5 which indicates that, except for two data points which were also excluded by Tomiyoshi in his analysis our calculated results are in good agreement with the experimental data.

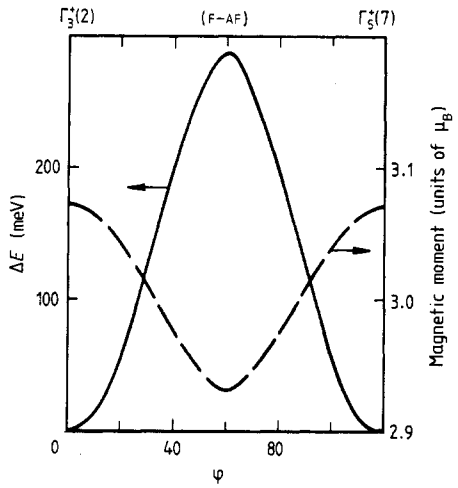

Figure 4. Total-energy differences per unit cell and Mn magnetic moments as a function of the angle ϕ leading from the state $\Gamma_3^+(\phi = 0°)$ to Γ_5^+ (No 7) ($\phi = 120°$). Except for Γ_3^+ and Γ_5^+ all states have a ferromagnetic component, but only the state (F-AF) of symmetry Γ_6^+ is self-consistent.

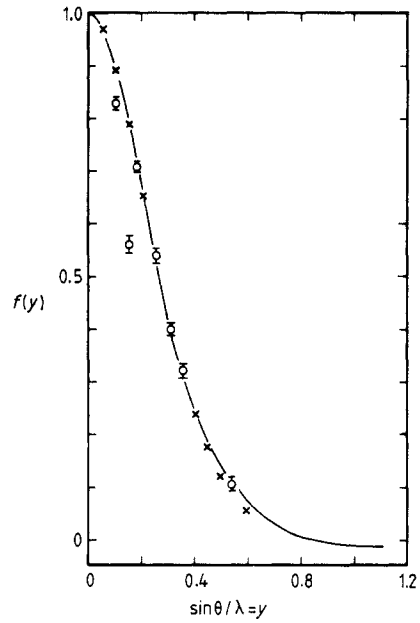

Figure 5. Calculated form factor of Mn in Mn_3Sn using the ground-state spin densities (curve), experimental values from Tomiyoshi (1982) (open circles), and Mn^{2+} data from Watson and Freeman (1961) (crosses).

Quite recently Ohmori *et al* (1987) found a long-period magnetic structure at low temperatures propagating along the *c* axis while keeping the spin arrangment—presumably of Γ_5^+ symmetry—in the planes perpendicular to the *c* axis; they state the period to be 12*c* and the magnitude of the magnetic moment to be $2.75\mu_B$/Mn. Although this latter value is nearly within the range of our calculated values, see table 2, the screw-spin structure poses new problems which are presently beyond our computational capabilities.

Another aspect of the experimental results is the existence of a weak ferromagnetic component below the Néel temperature of approximately $0.01\mu_B$ per unit cell. Tomiyoshi and Yamaguchi (1982) state that this is not due to the non-stoichiometry of the compounds, but arises from a distortion of the triangular spin structure. In fact, the distortion proposed is easily visualised by considering the action of a magnetic field along the spin direction of the atoms C in figure 2, state Γ_5^+ (No 7), which will slightly twist the spin direction of the four atoms A and B. Of course, a glance at figure 4 shows that such a distortion costs energy and will not be stable when the magnetic field is turned off. But the very same mechanism that will lift the degeneracy of the states Γ_3^+ and Γ_5^+ (No 7) may also alter the energetics slightly; this is presumably spin–orbit coupling (SOC) as embodied in Dzyaloshinsky (1958) and Moriya (1960a, b) exchange that was proposed by Tomiyoshi and Yamaguchi (1982) to be effective in this compound. That the energy changes brought about by SOC are indeed small, but not negligible, on the energy scales of figures 3 and 4 can be demonstrated in two special cases. These concern calculations including SOC for the collinear ferromagnetic and

antiferromagnetic spin structures labelled Γ_2^+ and Γ_4^- in figure 3(*b*), the former being shifted by SOC towards lower energy by 90 meV per unit cell, the latter by 70 meV per unit cell.

Returning to less delicate questions we now want to make an attempt to shed some light on the physical mechanism that gives rise to the large energy differences exposed in figures 3 and 4.

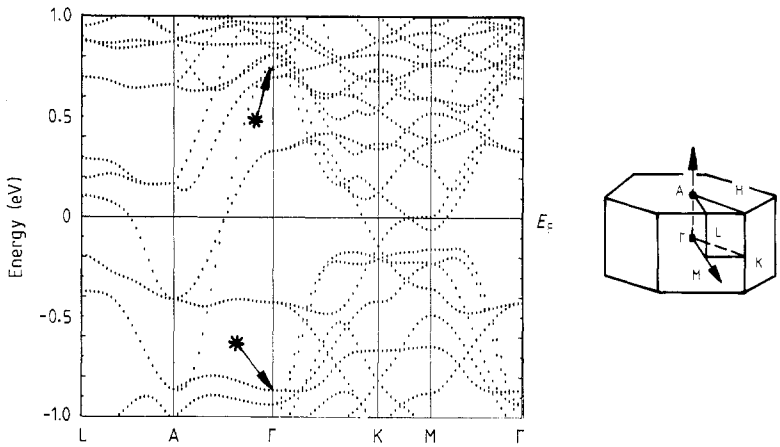

Figure 6. Band structure of Mn_3Sn in the low-total-energy state Γ_3^+ near the Fermi energy, E_F. Asterisks are explained in the text.

Considering the geometries of the spin arrangements shown in figure 2 one immediately sees that figure 3(*a*) reflects purely *inter-plane* exchange energies whose sign is thus seen to be ferromagnetic, whereas figure 4 reflects *intra-plane* exchange which is seen to be antiferromagnetic. The band structure of the low-total-energy state Γ_3^+ (or any other degenerate state—see table 2) is shown near the Fermi energy, E_F, in figure 6, that of the high-total-energy state Γ_1^- is shown in figure 7.

The different magnetic states are seen to possess completely different band structures, but one structure can be transformed into the other by a rotation through the angle ϕ as in figure 3(*a*). Thus in figure 7 one can follow the band states at $\Gamma(\boldsymbol{k} = 0)$ and see them change when going from the low-total-energy state Γ_3^+ to the high-total-energy state Γ_1^-. While the symmetry of the state Γ_1^- requires all band states to be at least twofold (spin) degenerate, because the sublattices A have opposite spin, and so do, separately, the sublattices B and C, the spin degeneracy is partially lifted in the state Γ_3^+ where the sublattices A have parallel spins and, similarly, for B and C (see figure 2). Most conspicuous is the behaviour of the state marked with asterisks which is split in the state Γ_3^+ by $\sim$ 1.5 eV. The wavefunctions of the split state consist of Sn p_z states plus Mn *xz* and *yz* on one plane combined symmetrically in case of the lower state or antisymmetrically in case of the upper state with Sn p_z and Mn *xz*, *yz* states on the other plane. This splitting (which one might call covalent) obviously lowers the total energy, furthermore, comparing figure 6 with figure 7, it quite effectively separates the states near the Fermi energy, E_F, lowering majority states below and rising minority states above E_F. The combined effect of this is a larger magnitude of the magnetic

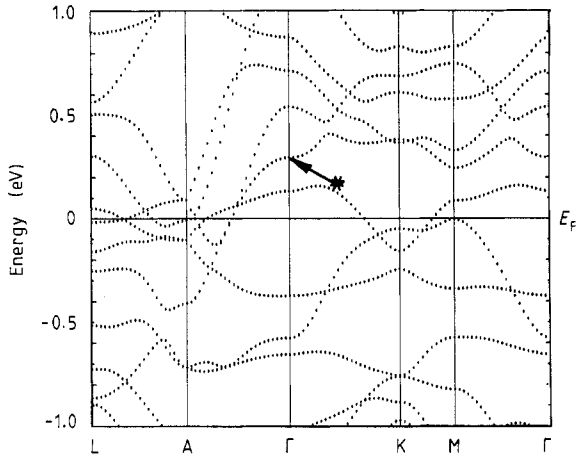

Figure 7. Band structure of Mn_3Sn in the high-total-energy state Γ_1^- near the Fermi energy, E_F. The asterisk is explained in the text.

moment in the low-total-energy state Γ_3^+ when compared with the high-total-energy state Γ_1^-, see also figure 3(*a*), where the magnetic moment is shown as a broken curve. Of course, the larger magnetic moment gives rise to a lower total energy which is roughly $-\frac{1}{4}I\mu^2$, where I is the intra-atomic exchange energy, typically of order of $\frac{1}{2}$ eV, and μ is the magnetic moment in multiples of μ_B. The connection between covalency, magnetic moment changes and the total energy has been discussed before by Kübler *et al* (1983) for the case of Heusler alloys.

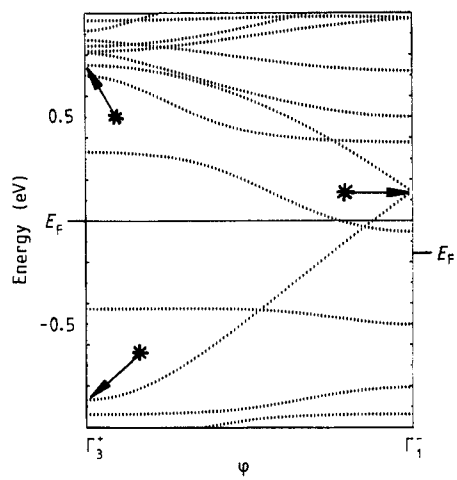

Figure 8. Band energy of the state at $\Gamma(\boldsymbol{k} = 0)$ as a function of the angle ϕ as in figure 3(*a*). The asterisks above Γ_3^+ mark the states similarly denoted in figure 6, that above Γ_1^- marks the state similarly denoted in figure 7.

Finally, the antiferromagnetic intra-plane exchange energy can also be made plausible using band structure data. Thus, when one moves from the left or right in figure 4

towards the ferromagnetic state (F–AF) at the centre, all remaining spin degeneracies will be lifted in figure 6, in particular, with reference to figure 8, the huge splitting marked at the left with the two asterisks decreases and the states at +0.3 eV and −0.43 eV split up into four states bringing majority states up towards the Fermi energy and minority states down. The ensuing decrease of the magnetic moment is apparent in figure 4 and gives rise to the higher total energy.

We thus conclude that our calculations revealed the reason for the energetics of the large trends of the possible magnetic structures in Mn_3Sn, finer details, however, that distinguish the states of low total energy, can only be resolved when our calculations include both the effects of non-collinearity and spin–orbit coupling. Calculations along these lines are underway.

Acknowledgments

Work was supported by the DFG under SFB 252 Darmstadt, Frankfurt, Mainz.

References

Dzyaloshinsky I 1958 *J. Phys. Chem. Solids* **4** 241–55
Haines E M, Heine V and Ziegler A 1985 *J. Phys. F: Metal Phys.* **15** 661–74
Hohenberg P and Kohn W 1964 *Phys. Rev.* B **136** 846–71
Kohn W and Rostoker N 1954 *Phys. Rev.* **94** 1111–20
Kohn W and Sham L J 1965 *Phys. Rev.* A **140** 1133–8
Korenman V, Murray J L and Prange R E 1977 *Phys. Rev.* B **16** 4048–57
Korringa J 1947 *Physica* **13** 392–400
Koster G F, Dimmock J O, Wheeler G, and Statz H 1963 *Properties of the 32 Point Groups* (Cambridge, MA: MIT Press)
Kouvel J S and Kasper J S 1964 *Proc. Int. Conf. Magnetism, Nottingham (1964)* (London: IOP) pp 169–70
Kübler J, Williams A R and Sommers C B 1983 *Phys. Rev.* B **28** 1745–55
Kübler J, Höck K-H, Sticht J and Williams A R 1988a *J. Phys. F: Metal Phys.* **18** 469–83
—— 1988b *J. Appl. Phys.* **63** 3482–6
Liechtenstein A I, Katsnelson M I, Antropov V P and Gubanov V A 1987 *J. Magn. Magn. Mater.* **67** 65–74
Lovesey S W 1984 *Theory of Neutron Scattering from Condensed Matter* vol 2 (Oxford: Clarendon)
Moriya T 1960a *Phys. Rev.* **117** 635–47
—— 1960b *Phys. Rev.* **120** 91–8
Nagamiya T 1979 *J. Phys. Soc. Japan* **46** 787–92
Oguchi T, Terakura K and Hamada N 1983 *J. Phys. F: Metal Phys.* **13** 145–60
Ohmori H, Tomiyoshi S, Yamauchi H and Yamamoto H 1987 *J. Magn. Magn. Mater.* **70** 249–51
Pindor A J, Staunton J, Stocks G M and Winter H 1983 *J. Phys. F: Metal Phys.* **13** 979–89
Sandratskii L M and Guletskii P G 1986 *J. Phys. F: Metal Phys.* **16** L43–8
Tomiyoshi S 1982 *J. Phys. Soc. Japan* **51** 803–10
Tomiyoshi S and Yamaguchi Y 1982 *J. Phys. Soc. Japan* **51** 2478–86
Tomiyoshi S, Yoshida H, Ohmori H, Kaneko T and Yamamoto H 1987 *J. Magn. Magn. Mater.* **70** 247–8
Vignale G and Rasolt M 1988 *Phys. Rev.* B **37** 10685–96
von Barth U 1984 *Many-Body Phenomena at Surfaces* ed. D Langreth and H Suhl (New York: Academic)
von Barth U and Hedin L 1972 *J. Phys. C: Solid State Phys.* **5** 1629–42
Watson R E and Freeman A J 1961 *Acta Crystallogr.* **14** 27–37
Williams A R, Kübler J and Gelatt C D Jr 1979 *Phys. Rev.* B **19** 6094–118
You M V and Heine V 1982 *J. Phys. F: Metal Phys.* **12** 177–94
Zimmer G J and Krén E 1972 *Magnetism and Magnetic Materials* (AIP Conf. Proc. No 10) (New York: AIP) pp 1379–83